

Reductive immobilization of $^{99}\text{Tc(VII)}$ by FeS_2 : the effect of marcasite

Rodriguez Hernandez, D. M.; Mayordomo, N.; Schild, D.; Shams Aldin Azzam, S.;
Brendler, V.; Müller, K.; Stumpf, T.;

Originally published:

May 2021

Chemosphere 281(2021), 130904

DOI: <https://doi.org/10.1016/j.chemosphere.2021.130904>

Perma-Link to Publication Repository of HZDR:

<https://www.hzdr.de/publications/Publ-32454>

Release of the secondary publication
on the basis of the German Copyright Law § 38 Section 4.

CC BY-NC-ND

1 Reductive immobilization of $^{99}\text{Tc(VII)}$ by 2 FeS_2 : the effect of marcasite

3
4 *Diana M. Rodríguez*¹, *Natalia Mayordomo*^{1*}, *Dieter Schild*², *Salim Shams Aldin Azzam*¹, *Vinzenz*
5 *Brendler*¹, *Katharina Müller*^{1*}, *Thorsten Stumpf*¹

6
7 ¹ Helmholtz-Zentrum Dresden – Rossendorf (HZDR), Institute of Resource Ecology, Bautzner
8 Landstraße 400, 01328 Dresden, Germany

9 ² Karlsruhe Institute of Technology (KIT), Institute for Nuclear Waste Disposal, Hermann-von-
10 Helmholtz-Platz 1, 76344 Eggenstein-Leopoldshafen, Germany

11 * Corresponding author: n.mayordomo-herranz@hzdr.de (N. Mayordomo, Phone: +49 351 260 2076),
12 k.mueller@hzdr.de (K. Müller, Phone: +49 351 260 2439)

13 14 ABSTRACT

15
16 Reductive immobilization of ^{99}Tc by a synthetic FeS_2 mixture, i.e. marcasite-pyrite 60:40, was studied
17 by a combined approach of batch experiments and powder X-ray diffraction, X-ray photoelectron
18 spectroscopy as well as Raman microscopy. It was found that the FeS_2 mixture removes 100% of Tc from
19 the suspension after 7 days in contact at $6.0 < \text{pH} \leq 9.0$. The retention outside that pH range was slower
20 and incomplete. Spectroscopic analysis showed that the redox active species at pH 6.0 is Fe^{2+} as expected
21 from previous works with pyrite. However, at pH 10.0 the surprising oxidation of S^{2-} to SO_4^{2-} was found
22 responsible for Tc immobilization. This was explained by the high reactivity of marcasite that is easily
23 oxidized to produce H_2SO_4 . Our work provides new molecular insights into the reductive mobilization
24 of Tc(VII) by oxidative formation of sulfate. The assigned molecular reactions may also be relevant for
25 the assessment of other redox reactive contaminants. Technetium re-oxidation experiments showed that
26 the fast oxidation of marcasite is associated to the reduction of the remaining Tc(VII) in solution, which
27 gives marcasite the potential of Tc natural remediation since it delays the re-oxidation of Tc(IV).

28
29 **KEYWORDS:** Technetium removal, iron sulfide, iron sulfate, pyrite, remediation

30

31 1. INTRODUCTION

32

33 Technetium (Tc, Z=43) was discovered in Italy by Perrier and Sagré in 1937.¹ Its application as a clinical
34 tracer element was first published in the early 60's.² Since then, the metastable ^{99m}Tc (half-life of 6.007 h)
35 has been used for the detection of tumors, as well as for the imaging of several organs like the brain or
36 the liver. Despite its relevance in medicine, technetium is very problematic from the environmental point
37 of view. The primary isotope, i.e. ⁹⁹Tc, a pure β^- emitter with a half-life of 2.14×10^5 years, is produced
38 with a high yield of 6% during the fission of ²³⁵U and ²³⁹Pu.³ Even though it may be naturally formed in
39 trace amounts through the spontaneous fission of ²³⁸U or the interaction of cosmic rays with
40 molybdenum, ruthenium and niobium present in the Earth crust, the vast majority of the technetium
41 present on our planet originates from human activities, like nuclear power production.^{3,4}

42

43 In addition to its long half-life, complex ⁹⁹Tc speciation adds to its high environmental risk. Under
44 oxidizing conditions it is mainly occurring as pertechnetate, Tc(VII)O₄⁻, an anion that is practically not
45 sorbed by minerals or sediments, and also does not form insoluble compounds.⁵ Thus, it freely migrates
46 within ground water.^{3,4} If Tc reaches the biosphere, it will be rapidly incorporated into the food chain
47 and when Tc dose exceeds 0.04 mSv per year (equivalent to the intake of 182 μ g of Tc), it can increase
48 the risk of cancer as well as other health problems related to radiation exposure.⁶ Therefore, establishing
49 strategies for pertechnetate immobilization and remediation is of great importance for the nuclear waste
50 management and environmental protection. The most stable species under reducing conditions is
51 Tc(IV)O₂, a scarcely soluble oxide with a very low mobility. Consequently, a reduction of TcO₄⁻ to TcO₂
52 is the most viable strategy for technetium immobilization.^{3,7,8} Several minerals containing different
53 reducing moieties like Sn(II)^{9,10} or Fe(II)¹¹⁻¹⁵ have been proven to effectively scavenge Tc from solution
54 through the formation of Tc(IV) and its consecutive precipitation, sorption and/or incorporation.

55

56 Pyrite, cubic iron sulfide (FeS₂), has shown a remarkable ability for the remediation of pollutants such
57 as mercury,¹⁶ chromium^{17,18} and molybdenum.¹⁹ In a recent study, we have found that it removes almost
58 100% of Tc(VII) from solution after one day in contact at $5.5 \leq \text{pH} \leq 10.5$.²⁰ X-ray absorption
59 spectroscopy, XAS, showed that after the reduction from Tc(VII), Tc(IV) was either sorbed onto hematite
60 (α -Fe(III)₂O₃) at pH 6.0 or incorporated into magnetite (Fe(II)Fe(III)₂O₄) at pH 10.0, with both hematite
61 and magnetite being oxidation products of pyrite. Based on these results, we concluded that natural
62 attenuation of Tc is expected in nuclear waste repositories with clays (namely bentonite) used as backfill

63 materials, where pyrite is a very common accessory mineral.²¹⁻²³ This is in particular relevant in sites
64 like the Onkalo spent nuclear fuel repository, where pyrite is abundant per se.²⁴ However, these natural
65 attenuation effects clearly depend on the interaction between technetium and other minerals present,
66 possibly changing the retention of Tc. Thus, more realistic scenarios like the presence of marcasite, a
67 FeS₂ polymorph commonly found along with pyrite in the environment,²⁵ should be taken into account.
68 Even though both minerals crystallize in different crystal systems, i.e. orthorhombic (marcasite) and
69 cubic (pyrite) and have different space groups (marcasite: Pnnm; pyrite: Pa $\bar{3}$), they are commonly
70 misidentified and confused based on mere crystal habit. For example, acicular pyrite crystals are
71 considered marcasite while in applications like jewelry it is very frequent that pyrite is sold as
72 marcasite.²⁶

73
74 It has been proven that polymorphism, i.e. the existence of a solid phase in different crystalline structures,
75 has a significant effect on the retention of pollutants by minerals. One example is europium sorption that
76 is faster on γ -alumina (γ -Al₂O₃) than on corundum (α -Al₂O₃) because the reaction rates are influenced
77 by the crystallographic features of the mineral.²⁷ The same effect has been observed for plutonium
78 sorption on hematite and maghemite (γ -Fe₂O₃).²⁸ Thus, it is quite probable that the retention of pollutants
79 by natural pyrite is affected by the presence of marcasite; however, no studies addressed this so far. More
80 specifically for technetium, retained Tc(IV) might get re-mobilized after the decomposition of marcasite,
81 that is unstable with respect to pyrite and whose main oxidation product, H₂SO₄, is a potential re-
82 oxidation agent for Tc(IV). Therefore, in order to design an efficient remediation strategy for Tc, a basic
83 understanding of the effect of marcasite on Tc immobilization by pyrite is needed.

84
85 In this work, we have studied the retention of Tc(VII) by a well characterized synthetic mixture of
86 marcasite-pyrite 60:40 using a combined approach of batch experiments with spectroscopic and
87 diffraction measures. The batch contact experiments were carried out at pH ranging from 4.0 to 10.5,
88 contact times from 1 to 45 days, and Tc concentrations varying from 0.1 μ M to 1 mM. X-ray
89 photoelectron spectroscopy (XPS), Raman microscopy and powder X-ray diffraction (XRD) were
90 applied to the Tc loaded solids to determine oxidation states and the mineralogical changes after the
91 interaction with technetium. Additionally, re-oxidation experiments were performed at pH 6.0 and 10.0
92 for 90 days, where Raman microscopy and XRD identified the reaction products.

93
94

95 2. MATERIALS AND METHODS

96

97 **Radiation safety.** ^{99}Tc is a β -particle emitter and should be handled only in a dedicated radiochemistry
98 laboratory with specific radiation safety protocols in place.

99

100 **General notes.** Unless indicated otherwise, all preparations were performed under N_2 atmosphere inside
101 a glovebox (GS Glovebox-System GS050912; < 1 ppm O_2) at 21°C . The Milli-Q water (resistivity of
102 $18.2 \text{ M}\Omega\cdot\text{cm}$, Water Purified[®]) used for the experiments was boiled for two hours for degassing, sealed
103 and cooled down to room temperature before its placement into the glovebox.

104

105 The Eh was measured with an Eh electrode (Inlab redox micro 51343203, Mettler Toledo) calibrated
106 with a redox buffer solution ($220 \text{ mV} / \text{pH } 7$). The pH was measured by using a pH meter (pH3110,
107 WTW) with a pH electrode (SI Analytics Blue Line) calibrated with standard pH buffers 4.006, 6.865
108 and 9.180 (WTW).

109

110 2.1 Mineral synthesis and characterization

111 Iron sulfide, FeS_2 , was synthesized in a Schlenk line following the procedure described by Huo et
112 al.²⁹ Briefly, 200 mL of 0.1 M FeCl_3 and 200 mL of 0.2 M NaHS were prepared and purged with N_2
113 for 30 minutes. Then, the solutions were mixed in a round flask of 500 mL and left under N_2
114 atmosphere and constant stirring for another 30 minutes. Lastly, the mixture was sealed and aged
115 for 24 hours in a stove at 60°C . The black powder obtained was separated by ultracentrifugation
116 (Optima XPN-80 Ultracentrifuge, Beckman Coulter at $2.4 \times 10^5 \times g$ for 1 hour, these conditions apply
117 for all centrifugations) and dried by lyophilization.

118

119 The characterization of the mineral is presented in the Supporting Information (Figure S1). It was
120 done by powder XRD (MiniFlex 600 powder XRD, Rigaku) using $\text{Cu K}\alpha$ ($\lambda = 1.54184 \text{ \AA}$) as X-ray
121 source with an X-ray generation of $40 \text{ kV} / 15 \text{ mA}$ (600 W) and a D/teX Ultra 1D silicon strip
122 detector in the Bragg-Brentano θ - 2θ geometry at a scanning speed of 0.02 deg per min . The samples
123 were prepared inside the glovebox, using an agate mortar to homogenize the solid and placing it into
124 a Kapton tape capped low-background airtight sample holders (Rigaku) to ensure inert N_2
125 conditions. The Brunauer-Emmett-Teller specific surface area was determined as $5.3 \pm 0.4 \text{ m}^2 \text{ g}^{-1}$,
126 using isotherm experiments with N_2 at 77 K (Multipoint Beckman Coulter surface analyzer SA
127 3100). The isoelectric point of the mineral (pH_{IEP}) was determined by zeta potential experiments

128 (Zetasizer Nano Series Nano-ZS, Malvern Instruments) of 0.05 g L⁻¹ mineral suspensions in 0.1 M
129 NaCl at pH values between 3.0 and 10.5. Each sample was scanned for 30 seconds; the data
130 presented here are averages of five independent scans. Scanning electron microscopy (SEM) was
131 used to analyze the mineral morphology. The sample was prepared inside the anoxic glovebox and
132 moved by a shuttle (Leica VCT) under inert conditions into the environmental scanning electron
133 microscope (FEI Quanta 650 FEG, now Thermo Fisher Inc.). The operating voltage was 30 kV and
134 the pressure in the analysis chamber 2.8×10⁻⁴ Pa.

136 2.2 Batch sorption experiments

137 All batch experiments started with the preparation of suspensions of the mixture marcasite-pyrite
138 60:40, from now on simply referred to synthesized FeS₂. In general, 42.6 mg of synthesized FeS₂
139 were suspended in water or 0.1 M NaCl (NaCl_(s) from Merck, purity ≥ 99%) depending on the
140 experiment. Afterwards, the indicated amount of a 9.22×10⁻³ M K⁹⁹TcO₄ stock solution (Institute of
141 Radiopharmaceutical Cancer Research, HZDR) was added. The final volume of the sample was
142 32 mL (final solid to liquid ratio = 1.3 ± 0.2 g L⁻¹). The pH of the samples was adjusted with
143 solutions from 1 to 0.02 M of HCl or NaOH. Due to the oxidation of FeS₂,³⁰ the pH was adjusted
144 regularly every 3 to 4 days adding small amounts of HCl or NaOH if required. Such additions never
145 exceeded 10 μL to ensure constant Tc concentration and ionic strength in the sample.

146
147 Once the pH was adjusted, the samples were placed on a horizontal shaker for agitation for the
148 required contact time. After this, the stirring was stopped and the pH and Eh were measured
149 (equilibrium time for Eh measure: 30 minutes). Table S1 in the supporting information (SI)
150 summarizes the conditions for the batch experiments.

151
152 The samples were then ultracentrifuged and 250 μL aliquots from the supernatant were taken to
153 measure the remaining Tc concentration by liquid scintillation counting, LSC (1414 LSC
154 Winspectral α/β Wallac, Perkin Elmer; detection limit: 0.42 Bq; measuring time: 10 minutes).

155
156 The amount of Tc retained by the synthesized FeS₂ (%Tc_{removed}) was calculated as follows:

$$157 \quad \%Tc_{removed} = \frac{([Tc]_0 - [Tc]_t)}{[Tc]_0} \times 100 \quad \text{Eq.1}$$

160 where $[Tc]_0$ is the initial Tc concentration in the system (in Bq mL⁻¹), measured in a blank solution
161 without the solid, and $[Tc]_t$ is the concentration of Tc remaining in solution after contact with the
162 synthesized FeS₂ (in Bq mL⁻¹) after certain time (t) of contact.

163

164 **2.3 X-ray photoelectron spectroscopy (XPS)**

165 0.140 g of the synthesized FeS₂ were transferred into 50 mL of water and the required amount of
166 K⁹⁹TcO₄ was added to obtain \approx 1000 ppm of Tc load in the final solid (Tc initial concentration =
167 0.048 mM). Such concentration was necessary to achieve at least 4 Tc atoms nm⁻², which is the value
168 needed to perform measurements. The pH was adjusted to 6.0 and 10.0 and the samples were left
169 for equilibration for a month on a horizontal shaker (the pH was also adjusted twice a week during
170 this month). Afterwards, the solid was separated by ultracentrifugation and the supernatant was
171 removed. The wet paste was re-dissolved in \approx 1 mL of water. Two blanks of synthesized FeS₂
172 suspensions in water (1.3 g L⁻¹) were prepared at pH 6.0 and 10.0, left in horizontal stirring for one
173 month adjusting the pH occasionally. They were measured at the same conditions as the ⁹⁹Tc-loaded
174 samples. The samples were always transported and measured under inert gas atmosphere (N₂ and
175 Ar).

176

177 A drop of the suspension was applied on indium foil and left to dry. Afterwards, the samples were
178 moved into the XPS (PHI 5000 VersaProbe II, ULVAC-PHI Inc.) using an airtight transfer vessel.
179 The XPS is equipped with a scanning microprobe X-ray source (monochromatic Al K α (1486.7 eV)
180 X-rays). X-ray source power of 32 W and pass energy of the analyzer of 187.85 eV were used to
181 perform survey scans of the conductive samples. Narrow scans of the elemental lines were recorded
182 at 23.5 eV pass energy, yielding an energy resolution of 0.67 eV FWHM at the Ag 3d_{5/2} elemental
183 line of pure silver. The binding energies of elemental lines of pure metals (monochromatic Al K α :
184 Cu 2p_{3/2} at 932.62 eV, Au 4f_{7/2} at 83.96 eV)³¹ were used for the calibration of the binding energy
185 scale of the spectrometer, obtaining an estimated error of \pm 0.2 eV.

186

187 **2.4 Raman microscopy**

188 Two suspensions of 1.3 ± 0.2 g L⁻¹ of the synthesized FeS₂ were prepared in water and their pH was
189 adjusted to 6.0 and 10.0. The required amount of K⁹⁹TcO₄ was added to obtain \approx 100 ppm of Tc
190 load in the final solid (Tc initial concentration = 5 μ M). Tc and the samples were placed on the

191 horizontal shaker for two weeks with regular pH adjustments. Afterwards, the solids were separated
192 by ultracentrifugation and distributed for Raman microscopy and powder XRD.

193
194 The wet paste was deposited on a cell containing two CaF₂ Raman quality windows.¹² Once the solid
195 was dry, the cell was sealed to ensure inert atmosphere during the measure. Raman microscopy
196 (Aramis, Horiba) was performed using a He – Ne laser (wavelength: 532 nm) with a 10-fold
197 objective with a D 0.3 filter, a pin-hole of 500 μm and a slit of 600 μm.

198 199 **2.5 Re-oxidation**

200 Two suspensions of the synthesized FeS₂ in water ($1.3 \pm 0.2 \text{ g L}^{-1}$) were prepared inside the glovebox
201 at pH 6.0 and 10.0, both containing 5 μM K⁹⁹TcO₄ (50 mL polypropylene tubes yielding a final
202 volume of 35 mL). They were agitated for 14 days during which the pH was regularly adjusted as in
203 the batch experiments (section 2.2). Subsequently, 3 mL aliquots of each sample were
204 ultracentrifuged and the supernatant was sampled for determination of Tc concentration remaining
205 in solution by LSC (section 2.2).

206
207 The tubes were opened outside the glovebox (under ambient atmosphere) and left with constant
208 stirring for one hour. Afterwards they were closed and placed on a horizontal shaker outside the
209 glovebox for 64 days. Identically to the batch experiments, we tried to adjust the pH, but this was
210 not possible as it always dropped to ~3 due to the production of H₂SO₄ after the oxidation of the
211 mineral³⁰ independent of the initial pH (6.0 or 10.0). Therefore, after two weeks adjusting every day,
212 we decided not to adjust the pH anymore but leave it at the stable value reached after the interaction
213 with oxygen (pH = 3.0 instead of 6.0 and pH = 2.8 instead of 10.0).

214
215 The suspensions were regularly sampled by taking 3 mL aliquots to measure the Tc remaining in the
216 supernatant by LSC (section 2.2). The solids obtained after 60 days of the re-oxidation experiments
217 were studied by powder XRD and Raman microscopy (sections 2.1 and 2.4).

218 219 **2.6 Speciation calculations**

220 Calculations were performed using the code Chess V2.4.³² The most recent Nuclear Energy Agency
221 thermodynamic databases for Fe^{33,34} and Tc³⁵ and their recommended S thermodynamic data were
222 used.

224 The reduction of 5 μM Tc(VII) by either S^{2-} or Fe^{2+} was studied as a function of pH. All calculations
225 assumed that the Tc(VII) reduction was promoted by either dissolved Fe^{2+} or S^{2-} at 25°C with no gas
226 dissolution. It was considered that 1% of 1.3 g L^{-1} FeS_2 was dissolved, i.e. 0.1 mM Fe^{2+} and 0.2 mM
227 S^{2-} . However, it has to be kept in mind that this assumption might not represent a realistic scenario
228 since Tc(VII) reduction is promoted by the structural S^{2-} or Fe^{2+} , whose redox potentials differ from
229 the dissolved ones when they form part of a mineral structure.^{36,37}

230

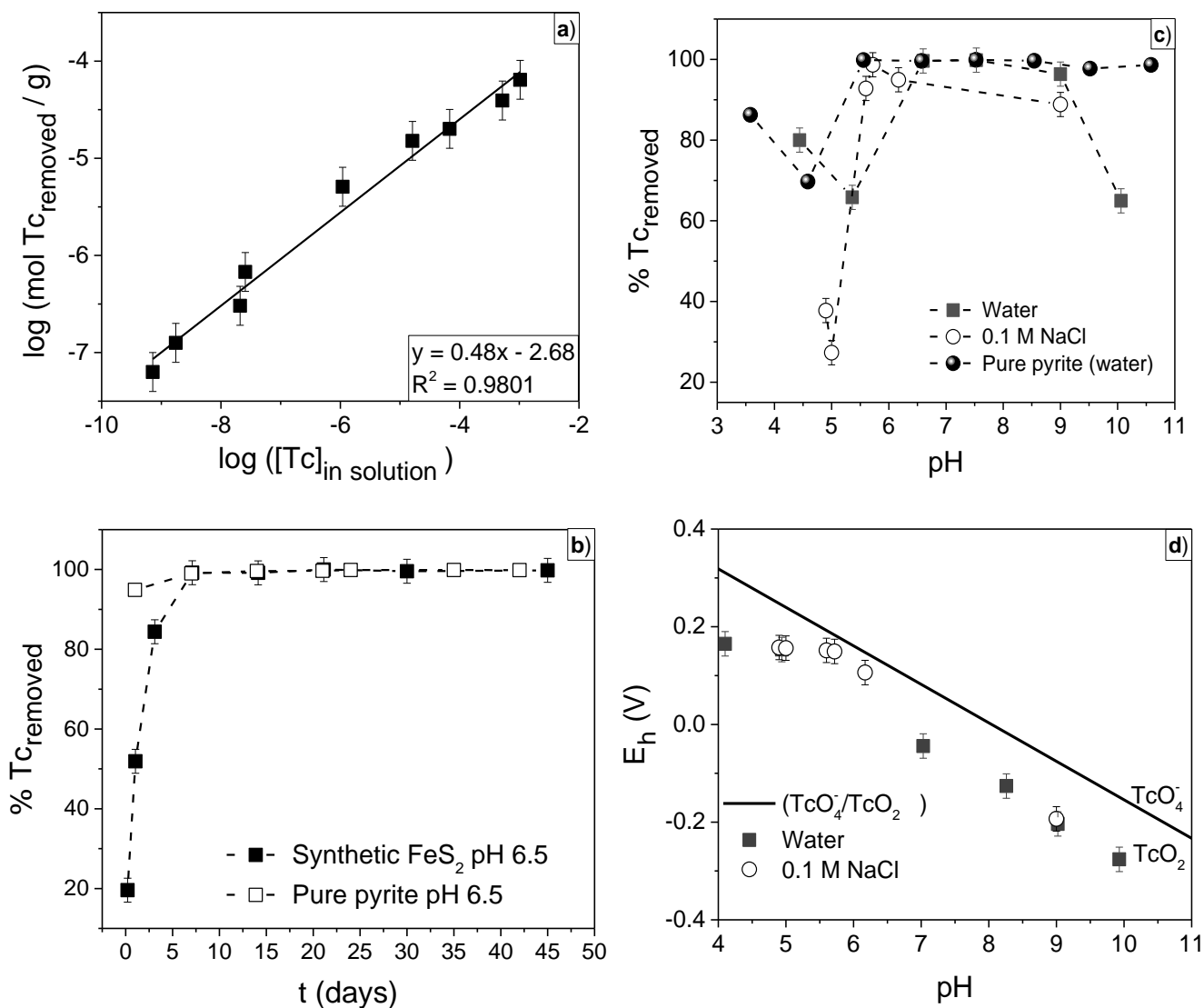
231 **3. RESULTS AND DISCUSSION**

232

233 **3.1 Batch sorption experiments**

234 Figure 1 shows the results of the batch experiments performed to study the $^{99}\text{Tc(VII)}$ uptake by the
235 synthesized FeS_2 as a function of Tc concentration, time and pH.

236



237

238

239

240

241

242

243

244

245

246

247

248

249

250

251

252

Figure 1. Batch experiments of $^{99}\text{Tc(VII)}$ removal by synthetic FeS_2 . a) Isotherm at pH 6.5 in water after 14 days of contact b) Scavenging kinetics at pH 6.5 in water. Tc removal by pure pyrite at pH 6.0 in water was added for comparison.¹⁵ c) Impact of ionic strength: water vs 0.1 M NaCl after 14 days in contact. Tc removal by pure pyrite in water for 14 days was added for comparison.¹⁵ d) Pourbaix diagram of the samples of c. Dashed lines in b and c are shown to guide the eye.

The isotherm at pH 6.5 (Figure 1a) shows that the lower the Tc concentration in suspension, the better its removal by the synthesized FeS_2 . These results are especially important because, due to technical reasons, for analyzing the kinetics of the removal process as well as the pH effect, we have used a Tc concentration of $5 \mu\text{M}$, which is three orders of magnitude higher than the typical technetium concentration in the environment ($1 \times 10^{-9} \text{ M}$).^{38,39} Therefore, the isotherm serves as a proof-of-concept of our experiments. Additionally, the isotherm shows a slope of 0.5 suggesting a single reaction mechanism, i.e. sorption on one site. This slope value indicates either that the affinity

253 of the mineral for the technetium is low,⁴⁰ or that the mechanism of removal could be the
254 precipitation of Tc(IV), most probably as TcO₂ or a TcS_x species.⁴¹

255

256 The kinetics of the Tc uptake at pH 6.5 are represented in Figure 1b. It can be seen that Tc removal
257 increases with time, with 50% of the initial technetium removed after one day in contact with the
258 synthesized FeS₂. 100% of Tc(VII) uptake was reached after 7 days. The experiment was carried out
259 for 45 days and the percentage of Tc(VII) scavenged was constant, showing no re-mobilization of
260 the radionuclei. Compared with the Tc immobilization by pure pyrite,²⁰ the presence of marcasite
261 slows down the process, since pure pyrite removed 100% of Tc already after one day of contact
262 under the same conditions.

263

264 Figure 1c shows that the removal of Tc(VII) from water at $6.0 < \text{pH} \leq 9.0$ is close to 100%. Under
265 more acidic conditions, the scavenging of technetium by the synthesized FeS₂ is less effective
266 because the solubility of FeS₂ increases as the pH decreases.⁴² It has been found that the
267 heterogeneous reduction of Tc(VII) by Fe(II) is more effective than the homogenous reduction (i.e.
268 in solution) since when Fe²⁺ as reducing agent is in solution the formation of Tc(IV) is kinetically
269 hindered.⁴³ In contrast, the reduction becomes more prominent when the Fe(II) takes part of a
270 mineral structure,^{29,43-45} or when it is pre-sorbed on a reactive mineral surface like on alumina.¹² In
271 our work, Tc removal at pH < 6.0 decreases due to FeS₂ dissolution, which hinders Tc(VII)
272 reduction.

273

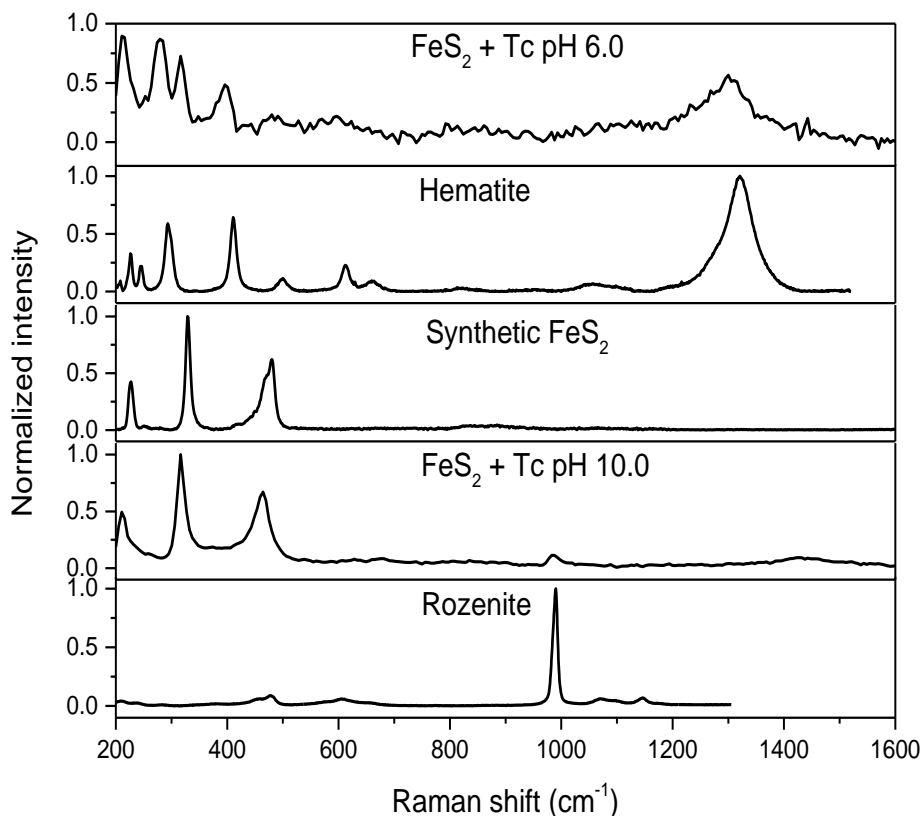
274 The Tc uptake by the synthesized FeS₂ also becomes lower at pH 10.0, which might be a result of
275 an increased solubility of TcO₂,^{11,46} or the formation of TcS_x-like compounds on the surface that
276 would passivate the mineral, preventing a further Tc reduction.⁴⁷ It has been reported that technetium
277 can passivate iron containing materials by forming layers of technetium oxides,^{48,49} however, in our
278 previous study of Tc retention by pure pyrite²⁰ such effect was not observed at pH 10.0 when
279 technetium interacted solely with oxygen, which lead us to conclude that if passivation is indeed
280 taking place, it would be most likely due to the formation of TcS_x and not TcO₂. The Pourbaix
281 diagram (Figure 1d) confirms the reduction from Tc(VII) to Tc(IV) in the whole pH range studied,
282 making the formation of both TcO₂ or TcS_x equally possible. One additional hint for a molecular
283 process understanding is given by the addition of 0.1 M NaCl to the retention system (Figure 1c).
284 As a consequence, the Tc removal at $6.0 < \text{pH} \leq 9.0$ does not significantly change, meaning that
285 inner-sphere complexation is likely taking place.⁵⁰ The difference on the Tc scavenging at pH < 6.0

286 between the system in water and 0.1 M NaCl can be explained either by outer-sphere complexation
287 or by the increase on Tc(IV) solubility as the ionic strength increases.^{11,51} In case that Tc(IV) is in
288 solution, its interaction with the synthesized FeS₂ would be hindered due to their charge repulsion.
289 Although batch experiments provided important macroscopic information, a combined approach of
290 spectroscopic and diffraction methods is needed for conclusions on the chemical identity of the Tc
291 species formed at the synthetic FeS₂ – water interface.

292

293 3.2 Molecular analysis of Tc loaded solids

294 To gain understanding on the retention on a molecular level, Raman microscopy and XPS were
295 performed on the solid samples after the interaction with technetium. The Raman spectra of the
296 solids at pH 6.0 and 10.0 are presented in Figure 2. At pH 6.0 the formation of hematite as the
297 resulting iron phase after the FeS₂ oxidation is confirmed by comparison of the spectra with the
298 reference R050300 of the RRUFF database.⁵² This result is in good agreement with our previous
299 findings with pyrite,²⁰ where the inner-sphere complexation of Tc(IV)-Tc(IV) dimers with hematite
300 was responsible of the Tc removal from solution at pH 6.0.



301
302
303
304
305

Figure 2. Raman spectra of Tc loaded (100 ppm) synthetic FeS₂ samples at pH 6.0 and pH 10.0. The spectra of the pure synthetic FeS₂ sample and reference spectra of hematite (reference R050300) and rozenite (FeSO₄×4H₂O, reference R070187) are shown for comparison.³⁰

306 Unlike the removal with pure pyrite,²⁰ the Raman spectra of the solid at pH 10.0 presents a band at
307 993 cm⁻¹ typical for the sulfate group of several Fe(II)-sulfate-hydrate minerals. As a reference
308 rozenite (Fe(II)SO₄·4H₂O) is shown in Figure 2. This band would indicate that the oxidation
309 reaction at this pH value is not that of iron, as expected for the Tc(VII) reductive immobilization,
310 but of sulfur. This is supported by the high spectral similarity of the Raman spectra of the Tc loaded
311 FeS₂ at pH 10.0 with the pure synthetic FeS₂. The band around 478 cm⁻¹ present in the synthesized
312 FeS₂ before and after the interaction with technetium can be assigned to the Fe(III) moieties⁵³
313 described in the mineral characterization presented in the Supporting Information.

314

315 Figure 3 shows the XPS spectra evaluated for Fe 2*p*, S 2*p*, O 1*s*, and Tc 3*d*. Figure 3a illustrates the
316 formation of Fe(III) at pH 6.0. In contrast, there is no significant change indicating the oxidation of
317 iron at pH 10.0. This supports the interpretation of Raman spectra (Figure 2) and confirms that at
318 pH 10.0 the main redox sensitive element of the synthesized FeS₂ is sulfur. However, the S 2*p* spectra
319 (Figure 3b) at pH 10.0 show no signal for sulfate, expected around 168 eV, whereas the binding
320 energies of Fe 2*p*_{3/2} (707.2 eV) and S 2*p*_{3/2} (162.5 eV) can be unequivocally assigned to FeS₂. This
321 can be explained by a significantly lower sulfate concentration below the XPS detection limit
322 concentration as result of the incomplete reduction of 5 μM Tc. Whereas XPS analyzes the sample
323 as a whole, the Raman microscope records spectra from different regions of interest of the mineral,
324 being able to detect minor components. As the formation of sulfate is the result of the
325 heteroreduction of technetium, it becomes clear why it could be detected by Raman microscopy in
326 specific spots of the sample but not by XPS. Moreover, the small intensity of the band at 993 cm⁻¹
327 in Figure 2 portrays the low concentration of sulfate present in the sample.

328

329 The O 1*s* spectra (Figure 3c) of the pure synthetic FeS₂ presents a signal around 532.3 eV that could
330 be assigned to adsorbed water, which has already been reported in literature for FeS₂.⁵⁴ After the
331 interaction with technetium, the samples at both pH 6.0 and 10.0 display the formation of similar
332 proportions of OH⁻ and O²⁻. The Tc 3*d* spectra of the solids at pH 6.0 and 10.0 are presented in
333 Figure 3d. Due to the low concentration of Tc in the experiments the speciation by XPS can only be
334 performed by the Tc 3*d* main lines. The presence of TcO₂ at both pH values is indicated by the Tc
335 3*d*_{5/2} peak at 256.5 eV, which is close to the reference value 256.8 eV.⁵⁵ The peak intensity suggests
336 that formation of TcO₂ is favored at pH 6.0.

337

338 More intriguing are the Tc $3d_{5/2}$ peaks around 254 eV, whose binding energy is close to the reference
339 binding energy for Tc(0) (253.9 eV⁵⁶). But it is preferably assigned to TcS_x or Tc-S-Fe bonding
340 because the complete reduction to metallic technetium is not probable, as can be seen in the next
341 paragraphs with the speciation calculations. A similar situation is noted in the Fe $2p$ spectra, where
342 the binding energy of Fe $2p_{3/2}$ at 707.2 eV (Figure 3a) is close to the reference values of FeS₂ at
343 707.3 eV⁴⁷ and Fe(0) at 707.0 eV⁵⁷ but it is assigned FeS₂ as it makes more chemical sense
344 according to the sample. Although a reference of the Tc $3d$ binding energy for TcS₂ could not be
345 found, the Tc $3d_{5/2}$ line of Tc₂S₇ has a binding energy of around 254.8 eV,⁵⁸ which is close to that of
346 the peaks around 254 eV in Figure 3c. In consequence, the peaks at 254 eV were assigned to the
347 formation of TcS_x-like species that seem to be more abundant as the pH becomes more alkaline.
348 Such species were not detected by the S $2p$ spectra due to the low concentration of technetium. In
349 section 3.1, it was suggested that TcS_x species could passivate the mineral making the Tc reduction
350 slower. Surface complexes might be formed, too, working as transient phases in the total redox
351 process. Further studies are needed to gain deeper insight.
352

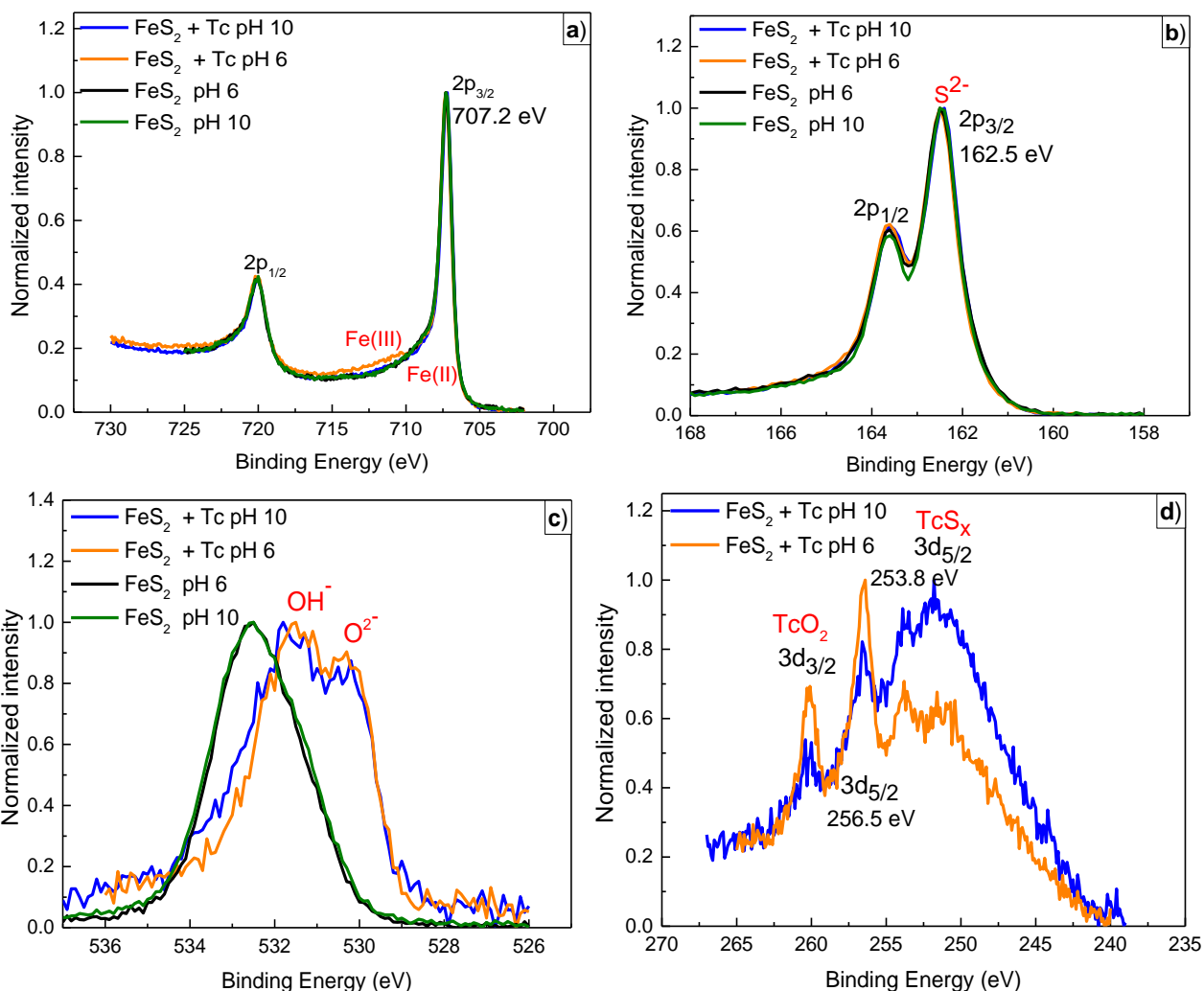


Figure 3. XPS spectra of the synthetic FeS₂ after the reaction with Tc(VII) ([Tc] = 1000 ppm) at pH 6.0 and 10.0. a) Fe 2p. b) S 2p. c) O 1s. d) Tc 3d. Tc 3d elemental lines are superimposed by the broad loss line of S 2s.

Figure S2 in the SI shows the speciation diagrams of Tc reduction in presence of Fe²⁺ and/or S²⁻. The performed calculations predict a quantitative Tc(VII) reduction to TcO₂ from pH 4.5 to pH 10.5. The Tc(VII) reduction by Fe²⁺ shows that main Fe(II) species in solution are Fe²⁺ at pH < 7.0 and for pH > 7.0 Fe(OH)⁺ and Fe(OH)₂. For Fe(III) the main species formed are hematite at pH < 6.5 and magnetite at pH > 6.5 (SI Figure S2a). In the case of the Tc reduction promoted by S²⁻, the main S(II) species are HS⁻ throughout the entire pH range evaluated and the sulfur oxidation products are S_(cr) at pH < 5.0 and SO₄²⁻ for pH > 5.0 (SI Figure S2b).

In contrast, when the reduction of Tc(VII) is calculated in presence of both Fe²⁺ and S²⁻ (SI Figure S2c), the formation of two solids, i.e. pyrite and mackinawite, and the presence of Fe²⁺_(aq), FeOH⁺_(aq) and HS⁻_(aq) are favored while the amount of Fe(III) and oxidized sulfur species represent a minority.

370 This is related to the fact that Fe^{2+} and S^{2-} concentration are respectively 20 and 40 times higher than
371 Tc and thus the main species found are Fe(II) and S(-II), whereas the formation of Fe and S oxidized
372 products is low in comparison. These set up conditions might not be representative for a realistic
373 scenario. However, when Fe^{2+} and SO_4^{2-} are in solution at $\text{pH} > 7.0$ the formation of FeSO_4 is
374 favored.⁵⁹ Even though these calculations need to be evaluated carefully since Tc homoreduction
375 (i.e. in solution) by Fe^{2+} and S^{2-} coming from an assumed 1% FeS_2 dissolution is assumed, they
376 support the Raman spectra obtained for the solids after interaction with Tc.

377

378 In summary, there is a clear effect of the marcasite on the technetium immobilization when compared
379 with the previous results obtained with pure pyrite.²⁰ Not only the overall process is slower but also
380 the Tc retention is incomplete at $\text{pH} 10.0$, which is a result of the change of the predominant redox
381 active element (sulfur instead of iron).

382

383 3.3 Re-oxidation experiments

384 The initial concentration of Tc was $5 \mu\text{M}$ and the systems were left to interact for 14 days, after
385 which the concentration of Tc in solution became $0.28 \mu\text{M}$ at $\text{pH} 6.0$ and $1.13 \mu\text{M}$ at $\text{pH} 10.0$. In
386 order to estimate the amount of oxygen necessary to oxidize the synthetic FeS_2 , the oxidation rates
387 previously published for marcasite⁶⁰ and pyrite⁶¹ were used. Assuming that the mineral was entirely
388 marcasite, the 0.065 g used for the re-oxidation experiments would need around 10 s to be fully
389 oxidized whereas if the sample was constituted only by pyrite, it would need around 6 days. Even
390 though these calculated times should be carefully considered as the FeS_2 oxidation rate should be
391 affected by the presence of Tc(VII) as an oxidizing agent, they allow us to conclude that the time of
392 the experiment was appropriate to observe Tc(IV) re-oxidation. Moreover, the concentration of
393 oxygen required was rapidly reached since the opened tubes were shaken for one hour, then closed
394 and left under constant agitation for the entire experiment and they were opened several times for
395 pH adjusting on the first days and for sampling during the following two months.

396

397 Figure 4 shows the results of the re-oxidation experiments. The batch experiments from Figure 4a
398 depict the interesting fact that after the suspension at $\text{pH} 10.0$ was in contact with ambient
399 atmosphere, the technetium concentration in solution was significantly lower ($0.48 \mu\text{M}$) than before
400 the opening of the tube ($1.13 \mu\text{M}$). It is important to bear in mind that marcasite is much more
401 reactive than pyrite and when it is exposed to oxidizing conditions, it rapidly generates H_2SO_4 .²⁶
402 This does not only explain the impossibility of maintaining the pH at 6.0 or 10.0 (section 2.5), but

403 is also responsible for the further reduction of the Tc(VII) that was still in the suspension before the
404 entry of oxygen at pH 10.0. The concentration of technetium in both suspensions remained below
405 1 μM for 50 days. In the last point of the re-oxidation experiments (64 days in figure 4a), it is
406 apparent that the re-oxidation begins and it is more favorable in the suspension initially set at pH 6.0
407 than at pH 10.0. This behavior is very similar to the one found for pure pyrite.²⁰ The slower re-
408 oxidation at pH 10.0 indicates that the Tc(IV)-species bond with the mineral is stronger, suggesting
409 surface complexation at pH 6.0 and incorporation or co-precipitation at pH 10.0.

410

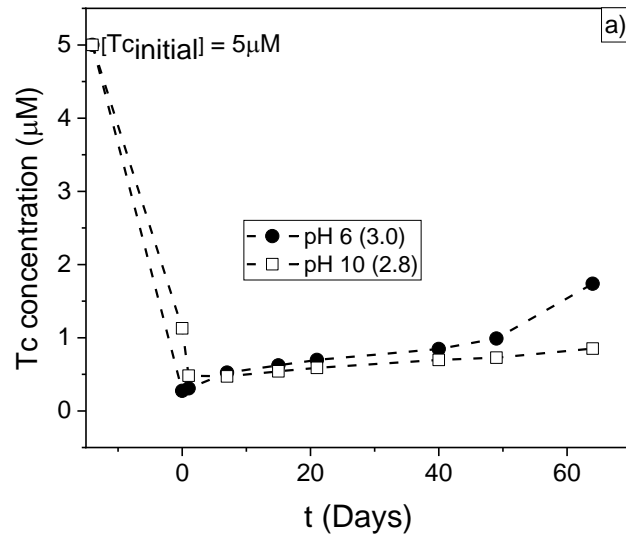
411 Figure 4b shows the Raman spectra of the two Tc loaded-solids after 50 days under ambient
412 atmosphere. The two solids have the same chemical identity, consisting of a mixture of the initial
413 mineral (marcasite-pyrite 60:40) and sulfur in solid state, whose presence was confirmed by XRD
414 of both solids (Figure 4c) and supported by the speciation calculations (SI Figure S2). This means
415 that the initial pH does not play a role on the speciation after the system interacts with oxygen, most
416 likely due to H_2SO_4 production.

417

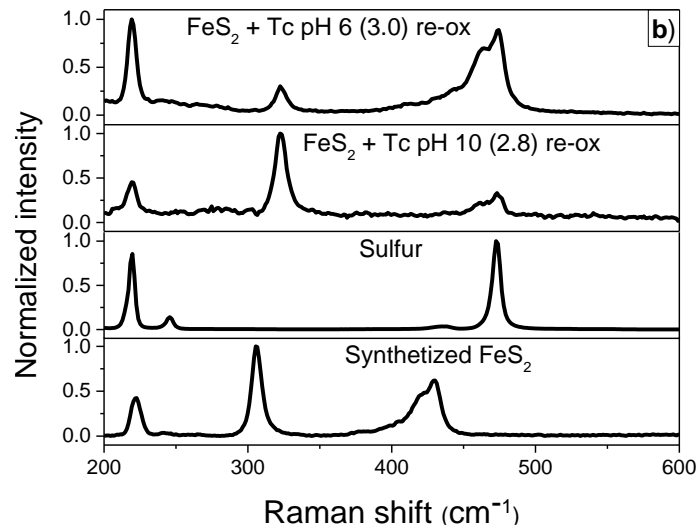
418 The results presented here show that the presence of marcasite along with pyrite in a nuclear waste
419 repository will prevent the re-mobilization of technetium due to the production of H_2SO_4 triggered
420 by the presence of O_2 and the subsequent formation of elemental sulfur. The oxidation of marcasite
421 is associated to the reduction of the Tc(VII) remaining in solution. Our results suggest that Tc will
422 be immobilized as Tc(IV) until all the marcasite has been consumed, which would considerably limit
423 a technetium distribution within the repository near and far field even if Tc(VII) reduction is not
424 complete.

425

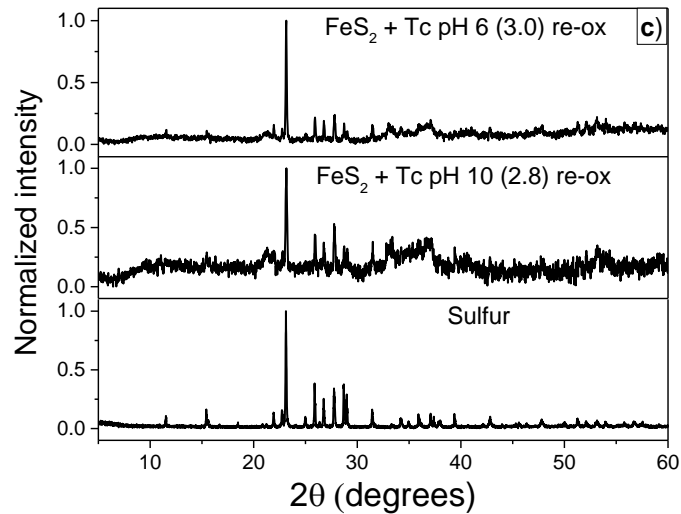
426



427



428



429 **Figure 4.** Evaluation of Tc re-oxidation (re-ox) experiments at different pH values (pH_{initial} = 6.0
 430 and 10.0; pH_{air} = 3.0 and 2.8, respectively). a) Tc concentration in suspension for 70 days in
 431 ambient atmosphere. Dashed lines are shown to guide the eye. b) Raman spectra of the solids at
 432 pH_{initial} 6.0 and 10.0 after 60 days of exposition to ambient atmosphere. The Raman spectra of the

433 pure synthetic FeS₂ and sulfur (reference R040135) are shown as reference.³⁰ c) XRD of the solids
434 at pH_{initial} 6.0 and 10.0 after 60 days of exposition to ambient atmosphere. The XRD of sulfur
435 (reference R040135) are shown as reference.³⁰

436

437 4. CONCLUSIONS

438 The immobilization of ⁹⁹Tc(VII) by a synthesized FeS₂, presenting a mixture of marcasite and pyrite
439 (60:40) was studied. It was found that 100% of Tc(VII) is removed from solution after 7 days of
440 interaction at 6.0 < pH ≤ 9.0. The Pourbaix diagram confirms that the initial step of the
441 immobilization is the reduction of Tc(VII) to Tc(IV) at all the working pH values. At pH < 6.0 the Tc
442 removal is incomplete due to the solubility of the synthesized FeS₂, as the reduction of Tc(VII) is less
443 efficient when Fe²⁺ is in solution. The spectroscopic analysis revealed that Fe(II) acts as the reducing
444 agent at pH 6.0, producing hematite on which Tc(IV) sorption is feasible. These results are
445 comparable to pure pyrite.²⁰ The behavior of the synthesized FeS₂ at pH 10.0 is different to pure
446 pyrite and very surprising. Here, the Raman spectra indicated the formation of a Fe(II)SO₄ like
447 mineral, implying that the reducing agent in that case was S²⁻, which is a consequence of the higher
448 reactivity of marcasite and might be an explanation for the incomplete Tc removal at this pH.
449 Previous works with mackinawite, FeS,⁶² and in the presence of microorganisms⁴⁷ have shown that,
450 in general, after the reduction of Tc(VII) the formation of TcS_x compounds and polysulfides is
451 observed. To our knowledge, our work provides new insights into the formation of sulfate minerals
452 after the reduction of Tc(VII), highlighting the importance of further studies of the interaction of
453 technetium with sulfur and other sulfur minerals like galena or chalcopyrite.

454

455 Even though the presence of marcasite makes the overall Tc retention less efficient when compared
456 with pure pyrite, the re-oxidation experiments showed that the production of H₂SO₄ under ambient
457 atmosphere leads to the immobilization of the technetium that was not retained by the synthesized
458 FeS₂. In a realistic scenario, the oxidation of marcasite will promote the Tc(VII) reduction, which
459 will favor Tc retardation due to the formation of less mobile Tc(IV) species.

460

461 As stated before, pyrite and marcasite are commonly misidentified and confused. This is a significant
462 problem for the modeling of their ability to immobilize contaminants in the environment, which is
463 especially important for most prominent redox-sensitive actinides and fission products in the context
464 of a nuclear waste repository. This study shows the crucial role of the crystalline structure in the
465 retention mechanism of technetium and opens the door to further comparisons of the scavenging

466 ability of other polymorphs, like hematite and maghemite. Likely, data sets of other environmental
467 pollutants, e.g. Se, As, Cd need a careful revision with respect to polymorphism.

468

469 **Supporting Information.** Conditions of the batch sorption experiments. Mineral characterization.
470 Speciations calculated as a function of pH.

471

472 **CRedit authorship contribution statement**

473 **Diana M. Rodríguez:** Formal analysis, Investigation, Writing - Original Draft. **Natalia Mayordomo**

474 **Herranz:** Formal analysis, Investigation, Writing - Review & Editing. **Dieter Schild:** Formal analysis,

475 Writing - Review & Editing. **Salim Shams:** Formal analysis, Writing - Review & Editing. **Vinzenz**

476 **Brendler:** Conceptualization, Writing - Review & Editing, Supervision, Project administration.

477 **Katharina Müller:** Conceptualization, Writing - Review & Editing, Supervision, Project administration.

478 **Thorsten Stumpf:** Conceptualization, Writing - Review & Editing, Supervision.

479

480 **Declaration of competing interest**

481 The authors declare that they have no known competing financial interests or personal relationships that

482 could have appeared to influence the work reported in this paper.

483

484 **Acknowledgments**

485 This work was supported by the German Federal Ministry of Economic Affairs and Energy (VESPA II
486 joint project; 02E11607B).

487 We are very grateful to Susana Jiménez, Stephan Weiß and Carola Eckardt for their help in the laboratory.

488

489 **References**

490 1 C. Perrier and E. Segrè, *Nature*, 1937, **140**, 193–194.

491 2 R. Herbert, P. W. Kulke and R. T. H. Shepherd, *Postgrad. Med. J.*, 1965, **41**, 656–662.

492 3 A. H. Meena and Y. Arai, *Environ. Chem. Lett.*, 2017, **15**, 241–263.

493 4 J. P. Icenhower, N. P. Qafoku, J. M. Zachara and W. J. Martin, *Am. J. Sci.*, 2010, **310**, 721–752.

494 5 K. H. Lieser and C. Bauscher, *Radiochim. Acta*, 1987, **42**, 205–213.

495 6 Environmental Protection Agency, *National Primary Drinking Water Regulations: Radionuclides*,
496 2000.

497 7 C. I. Pearce, R. C. Moore, J. W. Morad, R. M. Asmussen, S. Chatterjee, A. R. Lawter, T. G.

498 Levitskaia, J. J. Neeway, N. P. Qafoku, M. J. Rigali, S. A. Saslow, J. E. Szecsody, P. K.

499 Thallapally, G. Wang and V. L. Freedman, *Sci. Total Environ.*, 2019, **716**, 132849.

500 8 P. Gu, S. Zhang, X. Li, X. Wang, T. Wen, R. Jehan, A. Alsaedi, T. Hayat and X. Wang, *Environ.*
501 *Pollut.*, 2018, **240**, 493–505.

502 9 T. G. Levitskaia, S. Chatterjee, N. K. Pence, J. Romero, T. Varga, M. H. Engelhard, Y. Du, L.
503 Kovarik, B. W. Arey, M. E. Bowden and E. D. Walter, *Environ. Sci. Nano*, 2016, **3**, 1003–1013.

504 10 I. E. Johnson, S. Chatterjee, G. B. Hall, S. D. Burton, E. L. Campbell, M. A. Conroy, Y. Du, M.
505 S. Fujimoto, T. Varga, A. A. Kruger and T. G. Levitskaia, *Environ. Sci. Nano*, 2018, **5**, 890–903.

506 11 E. Yalçintaş, X. Gaona, M. Altmaier, K. Dardenne, R. Polly and H. Geckeis, *Dalt. Trans.*, 2016,
507 **45**, 8916–8936.

508 12 N. Mayordomo, D. M. Rodríguez, D. Schild, K. Molodtsov, E. V. Johnstone, R. Hübner, S. Shams
509 Aldin Azzam, V. Brendler and K. Müller, *J. Hazard. Mater.*, 2020, **388**, 122066.

510 13 M. S. Lee, W. Um, G. Wang, A. A. Kruger, W. W. Lukens, R. Rousseau and V. A. Glezakou, *Nat.*
511 *Commun.*, 2016, **7**, 1–6.

512 14 D. Boglalienko and T. G. Levitskaia, *Environ. Sci. Nano*, 2019, **6**, 3492–3500.

513 15 D. Boglalienko, O. Qafoku, R. K. Kukkadapu, L. Kovarik, Y. P. Katsenovich, D. E. Cherkasov, H.
514 P. Emerson and T. G. Levitskaia, *Environ. Sci. Nano*, 2021, **8**, 97–109.

515 16 Y. Sun, D. Lv, J. Zhou, X. Zhou, Z. Lou, S. A. Baig and X. Xu, *Chemosphere*, 2017, **185**, 452–
516 461.

517 17 T. Wang, T. Qian, L. Huo, Y. Li and D. Zhao, *Environ. Pollut.*, 2019, **255**, 112992.

518 18 Y. Li, X. Tian, J. Liang, X. Chen, J. Ye, Y. Liu, Y. Liu and Y. Wei, *Environ. Pollut.*, 2020, **264**,
519 114804.

520 19 N. Xu, C. Christodoulatos and W. Braida, *Chemosphere*, 2006, **62**, 1726–1735.

521 20 D. M. Rodríguez, N. Mayordomo, A. C. Scheinost, D. Schild, V. Brendler, K. Müller and T.
522 Stumpf, *Environ. Sci. Technol.*, 2020, **54**, 2678–2687.

523 21 O. Bildstein, L. Trotignon, M. Perronnet and M. Jullien, *Phys. Chem. Earth, Parts A/B/C*, 2006,
524 **31**, 618–625.

525 22 M. De Craen, M. Van Geet, L. Wang and M. Put, *Phys. Chem. Earth, Parts A/B/C*, 2004, **29**, 91–
526 103.

527 23 E. Gaucher, C. Robelin, J. M. Matray, G. Négrel, Y. Gros, J. F. Heitz, A. Vinsot, H. Rebours, A.
528 Cassagnabère and A. Bouchet, *Phys. Chem. Earth, Parts A/B/C*, 2004, **29**, 55–77.

529 24 M. Talikka, *Geological Mapping of the ONKALO Open Cut*, Posiva Oy, Olkiluoto, Finland, 2005.

530 25 X. Yao, F. Xia, A. P. Deditius, J. Brugger, B. E. Etschmann, M. A. Pearce and A. Pring, *Contrib.*
531 *to Mineral. Petrol.*, 2020, **175**, 27.

- 532 26 D. Rickard, *Sulfidic Sediments and Sedimentary Rocks*, Elsevier B.V, Amsterdam, 2012.
- 533 27 T. Baumer and A. E. Hixon, *J. Environ. Radioact.*, 2018, **195**, 20–25.
- 534 28 A. B. Khasanova, N. S. Shcherbina, S. N. Kalmykov, Y. A. Teterin and A. P. Novikov,
535 *Radiochemistry*, 2007, **49**, 419–425.
- 536 29 L. Huo, W. Xie, T. Qian, X. Guan and D. Zhao, *Chemosphere*, 2017, **174**, 456–465.
- 537 30 P. Bonnissel-Gissingier, M. Alnot, J.-J. Ehrhardt and P. Behra, *Environ. Sci. Technol.*, 1998, **32**,
538 2839–2845.
- 539 31 M. P. Seah, I. S. Gilmore and G. Beamson, *Surf. Interface Anal.*, 1998, **26**, 642–649.
- 540 32 J. van der Lee and L. de Wint, *Chess tutorial and Cookbook. Updated for version 3.0*, Ecole des
541 Mines de Paris, Fontainebleau, 1999.
- 542 33 R. J. Lemire, U. Berner, C. Musikas, D. A. Palmer, P. Taylor and O. Tochiyama, *Chemical*
543 *Thermodynamics of Iron. Part 1*, OECD Nuclear Energy Agency Data Bank, Paris, France, 2013,
544 vol. 13a.
- 545 34 R. J. Lemire, D. A. Palmer, H. Schlenz and P. Taylor, *Chemical Thermodynamics of Iron. Part 2*,
546 OECD Nuclear Energy Agency Data Bank, Boulogne-Billancourt, France, 2019.
- 547 35 I. Grenthe, X. Gaona, A. V. Plyasunov, L. Rao, W. H. Runde, B. Grambow, R. J. M. Konings, A.
548 L. Smith and E. E. Moore, *Second update on the chemical thermodynamics of uranium,*
549 *neptunium, plutonium, americium and technetium*, OECD Nuclear Energy Agency Data Bank,
550 Boulogne-Billancourt, France, 2020.
- 551 36 C. A. Gorski, R. Edwards, M. Sander, T. B. Hofstetter and S. M. Stewart, *Environ. Sci. Technol.*,
552 2016, **50**, 8538–8547.
- 553 37 F. Li, L. Tao, C. Feng, X. Li and K. Sun, *Environ. Sci. Technol.*, 2009, **43**, 3656–3661.
- 554 38 E. H. Schulte and P. Scoppa, *Sci. Total Environ.*, 1987, **64**, 163–179.
- 555 39 K. Shi, X. Hou, P. Roos and W. Wu, *Anal. Chim. Acta*, 2012, **709**, 1–20.
- 556 40 G. Limousin, J.-P. Gaudet, L. Charlet, S. Szenknect, V. Barthès and M. Krimissa, *Appl.*
557 *Geochemistry*, 2007, **22**, 249–275.
- 558 41 J. Rard, M. Rand, G. Anderegg and H. Wanner, *Chemical Thermodynamics of Technetium*, North
559 Holland Elsevier Science Publishers B. V., Amsterdam, The Netherlands, 1999.
- 560 42 F. King, *A review of the properties of pyrite and the implications for corrosion of the copper*
561 *canister Technical Report TR-13-19*, Svensk Kärnbränslehantering AB, Stockholm, Sweden,
562 2013.
- 563 43 D. Cui and T. E. Eriksen, *Environ. Sci. Technol.*, 1996, **30**, 2259–2262.
- 564 44 D. Cui and T. E. Eriksen, *Environ. Sci. Technol.*, 1996, **30**, 2263–2269.

565 45 J. M. Zachara, S. M. Heald, B.-H. Jeon, R. K. Kukkadapu, C. Liu, J. P. McKinley, A. C.
566 Dohnalkova and D. A. Moore, *Geochim. Cosmochim. Acta*, 2007, **71**, 2137–2157.

567 46 A. Baumann, X. Gaona, E. Yalçintaş, K. Dardenne, T. Prüßmann, J. Rothe, S. Duckworth, M.
568 Altmaier and H. Geckeis, *Appl. Geochemistry*, 2018, **98**, 321–330.

569 47 C. I. Pearce, J. P. Icenhower, R. M. Asmussen, P. G. Tratnyek, K. M. Rosso, W. W. Lukens and
570 N. P. Qafoku, *ACS Earth Sp. Chem.*, 2018, **2**, 532–547.

571 48 G. H. Cartledge, *Corrosion*, 1955, **11**, 23–30.

572 49 G. H. Cartledge, *J. Electrochem. Soc.*, 1971, **118**, 1752–1758.

573 50 P. C. Hiemenz and R. Rajagopalan, *Principles of Colloid & Surface Chemistry*, Taylor & Francis,
574 New York, 3rd edn., 1997.

575 51 N. J. Hess, Y. X. Xia, D. Rai and S. D. Conradson, *J. Solution Chem.*, 2004, **33**, 199–226.

576 52 B. Lafuente, R. T. Downs, H. Yan and N. Stone, in *Highlights in Mineralogical Crystallography*,
577 De Gruyter, Berlin, 2015, pp. 1–30.

578 53 M. Hanesch, *Geophys. J. Int.*, 2009, **177**, 941–948.

579 54 S. W. Knipe, J. R. Mycroft, A. R. Pratt, H. W. Nesbitt and G. M. Bancroff, *Geochim. Cosmochim.*
580 *Acta*, 1995, **59**, 1079–1090.

581 55 *NIST X-ray Photoelectron Spectroscopy Database, Version 4.1*, National Institute of Standards
582 and Technology (NIST), Gaithersburg, USA, 2012.

583 56 V. N. Gerasimov, A. G. Zelenkov, V. M. Kulakov, V. A. Pchelin, M. V Sokolovskaya, A. A.
584 Soldatov and L. V Chistyakov, *J. Exp. Theor. Phys.*, 1982, **55**, 205–208.

585 57 J. F. Moulder, W. F. Stickle, P. E. Sobol and K. D. Bomben, *Handbook of X-ray Photoelectron*
586 *Spectroscopy*, ULVAC-PHI, Inc. Japan, Physical Electronics USA, Inc., Eden Prairie, USA, 1995.

587 58 V. N. Gerasimov, A. G. Zelenkov, V. M. Kulakov, V. A. Pchelin, M. V. Sokolovskaya, A. A.
588 Soldatov and L. V. Chistyakov, *J. Exp. Theor. Phys.*, 1984, **59**, 683–688.

589 59 B. S. Hemingway, R. R. Seal and I.-M. Chou, *Thermodynamic Data for Modeling Acid Mine*
590 *Drainage Problems: Compilation and Estimation of Data for Selected Soluble Iron-Sulfate*
591 *Minerals Open-file Report 02-161*, U.S. Geological Survey, 2002.

592 60 M. J. Rinker, H. W. Nesbitt and A. R. Pratt, *Am. Mineral.*, 1997, **82**, 900–912.

593 61 M. A. Williamson and J. D. Rimstidt, *Geochim. Cosmochim. Acta*, 1994, **58**, 5443–5454.

594 62 E. Yalçintaş, A. C. Scheinost, X. Gaona and M. Altmaier, *Dalt. Trans.*, 2016, **45**, 17874–17885.